ACS OMEGA

Open Access

http://pubs.acs.org/journal/acsodf

Article

In Situ Formation of Hydrogel Wound Dressing Based on Carboxymethyl Chitin/Tannic Acid for Promoting Skin Wound Healing

Jinhui Lin, Siyaqi Li, Yunfei Ying, Weilin Zheng, Jingcheng Wu, Peiyuan Wang,* and Xiaolong Liu*

Cite This: *ACS Omega* 2024, 9, 4386−4394

Read Online

ACCESS | Metrics & More | Article Recommendations | Supporting Information

ABSTRACT: Triggering the healing process of drug-resistant bacteria-infected wounds has attracted great attention due to global morbidity that may induce gangrene, amputation, and even death. Here, a chitin derivative, carboxymethyl chitosan (CMC), tannic acid (TA), and Cu^{2+} were used for hydrogel engineering. Using sodium bicarbonate as the neutralizer and reductant, hydrogen bonds between CMC and TA and in situ $Cu(OH)_2$ generation via ion coordination force between Cu^{2+} and TA facilitated the synthesis of CMC/TA/Cu hydrogel. Cu^{2+} and TA release, cytotoxicity, in vitro cell migration, angiogenesis, and antidrug-resistant bacteria were measured. Besides, wound closure was evaluated in vivo using the methicillin-resistant *Staphylococcus aureus* (MRSA)-infected excisional dermal wound mouse model. Negligible toxicity was observed both in vitro and in vivo. Dermal cell migration and angiogenesis were significantly enhanced. In vivo, the CMC/TA/Cu hydrogel induced effective re-epithelialization, collagen deposition, inflammatory alleviation, and MRSA inhibition during wound repair in mice. All these results confirmed that the CMC/TA/Cu hydrogel is a promising novel dressing for chronic wound healing in clinic.

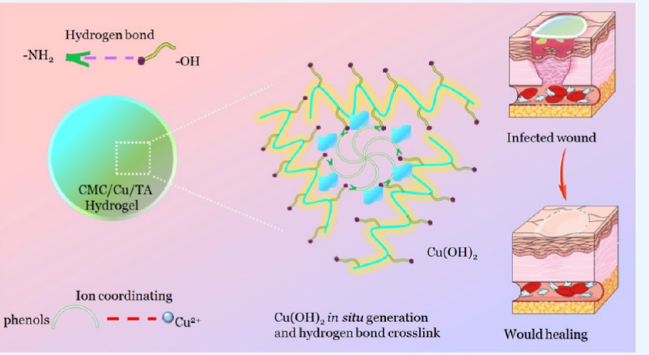

1. INTRODUCTION

Skin tissue is the largest organ in the human body; furthermore, it is essential for various bodily functions, which often include temperature control, hydration, and defense against external harm.[1,2] Unfortunately, lots of severe skin damages typically induced by burns, acute trauma, and chronic illness lead to uncontrollable bleeding, drug-resistant strain infections, and high extent of oxidative stress that might be life-threatening and cause a huge economic burden on clinical patients and the whole medical service system.[3,4] In recent years, hydrogel wound dressing has been widely explored for aiding in severe skin damage. Nevertheless, owing to the structural or functional defects, conventional dressing products, like gauze, plasters, or bandages, are confronted with the lack of simultaneous integration of microbial infection inhibition and acceleration of wound restoration.[5−8] Hydrogels, contrastively, are considered as optimal wound repair dressings on account of their highly moist microenvironment, biomimetic extracellular matrix, and antibacterial and microbial abilities for inhibition of wound infection.[9−11]

Due to the nontoxicity, desirable biodegradation, and positive bioactivity, hydrogels with the constitution of natural polymers have been extensively engineered for wound dressings. Among these biopolymers, by reason of the massive reserves in nature, chitin has been widely considered in the construction of wound healing hydrogels.[12−14] It is an ancient structural amino polysaccharide, and marine arthropods are its main source.[15−17] A large number of hydrophilic groups are found in the backbones of chitin, which endows it an ideal dressing for engineering of hydrogel systems with high swelling. The strong intermolecular or intramolecular hydrogen bonds in chitin, however, impend the solubility of water or other conventional organic solvents, resulting in the great limitation of the fabrication of chitin-based hydrogels..[18,19] Luckily, the chemical functionalization of chitin, like deacetylation, hydroxypropylation, and carboxymethylation, can make it become water soluble; therefore, chitin-originated hydrogels can be synthesized under mild conditions.[20] Carboxymethyl chitosan (CMC) can be obtained after the deacetylation and carboxymethylation of chitin. As one of the most important derivations of chitin, CMC-based hydrogel is considered as a specific polyampholyte dressing that possess both carboxyl (−COOH) and amino ($-NH_2$) groups, thereby

Received: September 5, 2023
Revised: December 20, 2023
Accepted: December 28, 2023
Published: January 16, 2024

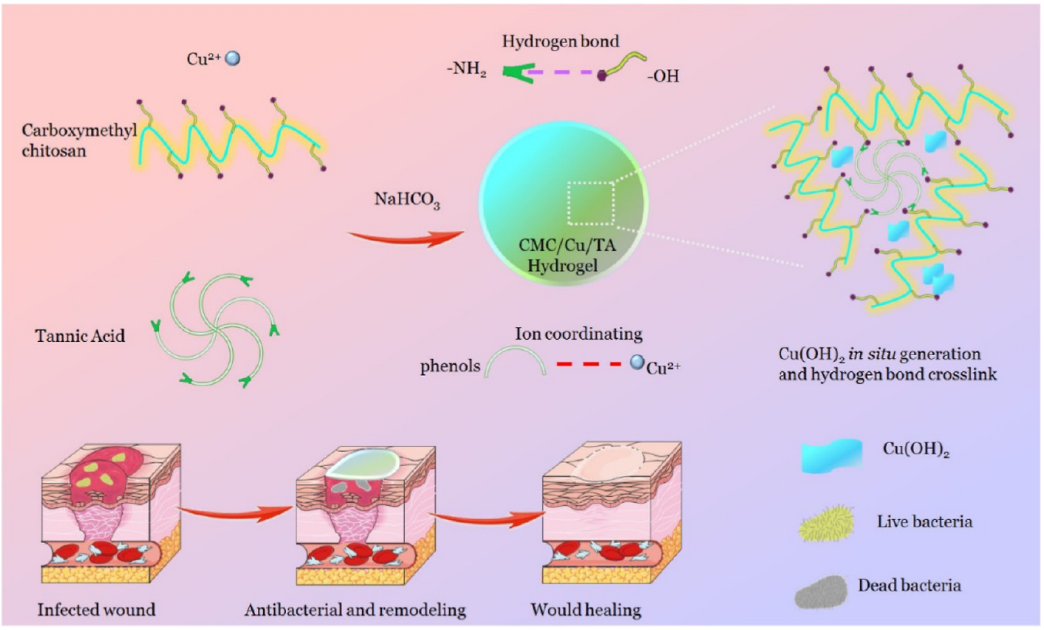

Figure 1. Schematic illustration of CMC/TA/Cu hydrogel fabrication for bacterial elimination and skin wound healing.

forming a cross-linked framework with positive charge, which can transform the charge state of ionic groups under varying pH microenvironment.[21] CMC is reported as a chemically adaptable biomedical material; as a result of its outstanding analogous biomedical properties, like degradability, antibacterial ability, and hemostatic effect, it has been broadly utilized in biomedicine, bioengineering, and drug delivery applications.[22−25] Nevertheless, the bacterial elimination effect still needed to be improved, particularly in the repair of multidrug-resistant bacteria-infected wounds.

Inspired by the free radical scavenging feature of polyphenols and the fact that polyphenols can enhance the mechanical properties of flour-based products, tannic acid (TA) is a kind of plant polyphenol that has already gained abundant attention in wound dressing applications.[26−29] Owing to the phenolic hydroxyl groups, it is able to easily link with lots of polymers via general noncovalent interactions, especially, hydrogen bonding.[30,31] Like other reported polyphenols, TA has antibacterial, antiviral, anticancer, and anti-inflammatory features.[32,33] Meanwhile, it possesses preventive properties against various diseases with initiation and progression via oxidative stress, like wound infection, inflammation, and cardiovascular ailments. Therefore, as the bioactive additive, TA has been investigated for tissue engineering and skin repair tasks.[34−36] Accordingly, the CMC/TA-based hydrogel might exhibit huge potential in promoting bacterial inhibition and would healing. Besides, phenolic hydroxyl groups from TA provide lone-pair electrons to coordinate with metal ions, including Fe^{3+}, Cr^{3+}, Mn^{3+}, and Cu^{2+}, etc.[37] Furthermore, great efforts have been spared for a synergistic antibacterial effect. According to previous reported studies, copper-based nanoagents with exceptional biocompatibility and efficacious sterilization have attracted substantial attention in wound healing.[38,39] Of particular interest is the utilization of Cu^{2+}, as it has been demonstrated to stimulate angiogenesis, accelerate the proliferation and migration of keratinocyte, and boost collagen deposition that prominently led to the amplification of the wound healing effect.[40,41] However, because of the microporous structure of the reported hydrogels, it remains a daunting challenge to quickly and uniformly anchor Cu^{2+} in wound dressing.

On these grounds, in this work, we have constructed a CMC and Cu^{2+}-based composite hydrogel via the bridging agent of TA. CMC could link with TA via hydrogen bonding, and Cu^{2+} was anchored with TA through powerful ion coordination. Sodium bicarbonate ($NaHCO_3$) was introduced for neutralization and ion reduction; thereafter, the CMC/TA/Cu hydrogel was constantly formed. Owing to the in situ generation of $Cu(OH)_2$ nanoparticles, potent growth, and migration of keratinocyte, angiogenesis of endothelial cells was observed in vitro. Besides, due to the forceful antibacterial abilities of the three counterparts, the multidrug-resistant strain of *Staphylococcus aureus* in the infected wound was rapidly ablated after treating with CMC/TA/Cu hydrogel in vivo (Figure 1). With the integration of nontoxic feature after local wound administration, the fascinating hydrogel can be further applied in the clinical therapy of drug-resistant strain-infected full-thickness wounds.

2. EXPERIMENTAL SECTION

2.1. Preparation of CMC. First, chitosan was obtained from the aqueous alkali solution (4050%) for deacetylation of α-chitin under 100−160 °C for a few hours. According to the strategy from Moores, the chitosan synthesized by this approach has deacetylation level up to 95%.[42] CMC synthesis was conducted under heterogeneous conditions including two steps (alkalization and etherification) using a double-wall cylindrical glass reactor equipped with a circulating-thermostat (25 ± 1 °C). Initially, 3 g of purified chitosan was added in 65 mL of isopropanol, and then 40% of NaOH aqueous solution was introduced into the reaction dropwise. The system was magnetically stirred at room temperature for 15 min. When alkalization completed, 6.0 mol of monochloroacetic acid dissolved in the same volume of isopropanol was introduced under gentle stirring, and the reacted system was stirred at room temperature for 10 h. Then, the solid sample was filtered and resuspended in methanol. After being neutralized by glacial acetic acid, the obtained product was filtered and

https://doi.org/10.1021/acsomega.3c06683
ACS Omega 2024, 9, 4386−4394

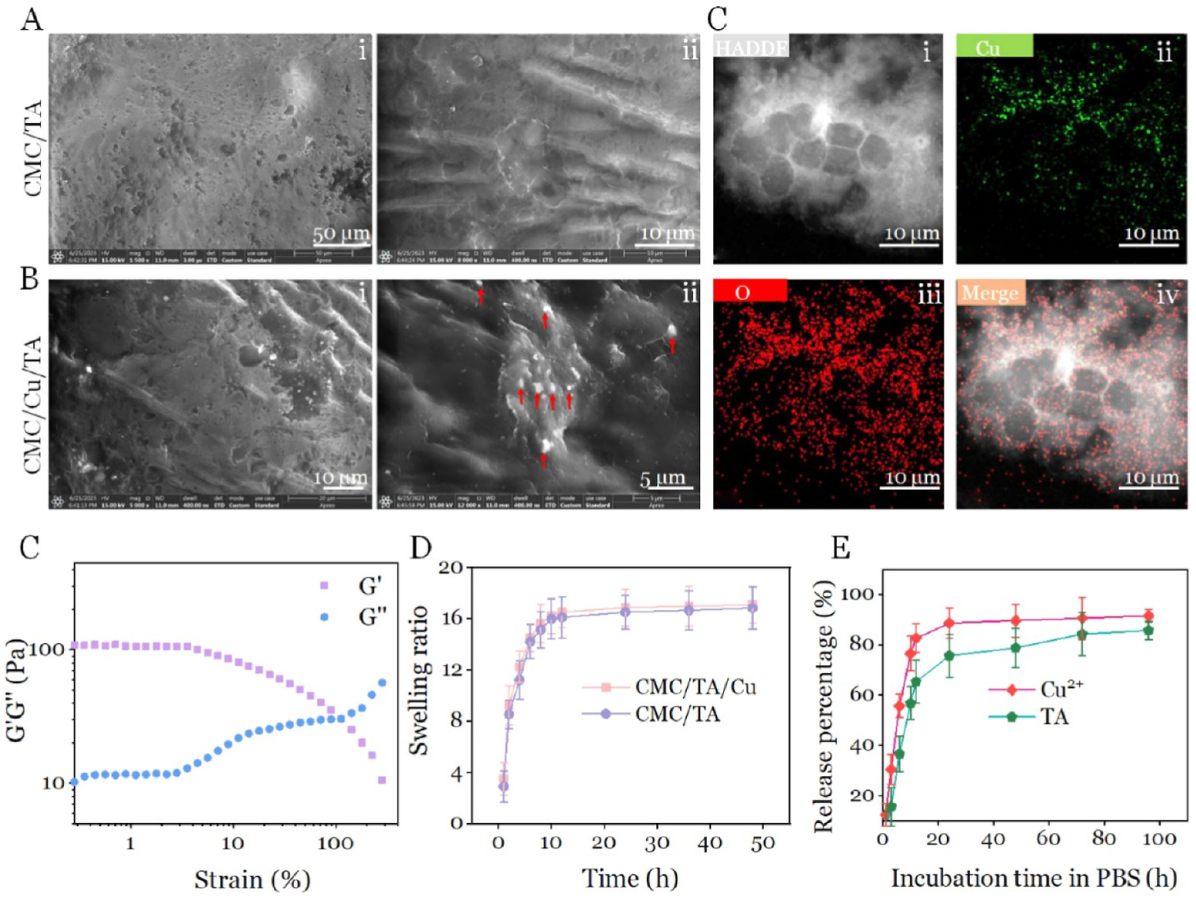

Figure 2. Morphologies of CMC/TA (Ai) and CMC/TA/Cu (Bi) hydrogels by using SEM. The magnified SEM images of CMC/TA (Aii) and CMC/TA/Cu (Bii) hydrogels. Red arrow refers to the in situ generated $Cu(OH)_2$ particles. (C) High-angle annular dark-field image and elemental mapping images of CMC/TA/Cu. (D) Strain amplitude sweep curve of CMC/TA/Cu. (E) Swelling ratios of CMC/TA and CMC/TA/Cu hydrogels. (F) Cu^{2+} and TA release profiles after immersing in CMC/TA/Cu in pH = 5.5 buffer for various periods.

extensively washed by 80% ethanol to dislodge the undesirable byproducts; finally, the CMC was dried at room temperature.

2.2. Preparation of CMC/TA/Cu Hydrogel. Typically, 5% (w/v) $CuCl_2$ aqueous solution, 4% (w/v) $NaHCO_3$ aqueous solution, 0.3 g/mL TA, and 5% (w/v) CMC solution were freshly prepared. Subsequently, 50 μL, 5% (w/v) of $CuCl_2$ and 50 μL, 4% (w/v) of $NaHCO_3$ solution were mixed together with 100 μL of the above TA solution. The mixed solution was shaken for 30 s at room temperature. Immediately, 250 μL, 5% (w/v) of CMC solution was introduced into above mixture to prepare the CMC/TA/Cu hydrogel (within 15 s).

2.3. Antibacterial Studies. For scanning electron microscopy (SEM) images of (methicillin)-resistant *S. aureus* (MRSA), two groups of MRSA (2 h immersion of PBS and CMC/TA/Cu) were first centrifuged by 0.9% NaCl three times and fixed for 30 min with 2.5% paraformaldehyde at 4 °C. Immediately, after being washed three times with 0.9% NaCl, all MRSA was stepwise dehydrated by using ethanol/water (v/v %, 30, 40, 50, 60, 70, 80, 90, and 100%). After the surface coating by gold spraying, the finally prepared bacterial products were detected under SEM. The SEM images of *Escherichia coli* were obtained by the same procedure.

2.4. Scratch Assay Studies. The human epithelial keratinocyte (HEK) cell scratch experiment is performed as follows: 5×10^5 per/well of HEK cells were first seeded at a 12-well plate and starved for 6 h, and the scratch wounds were immediately produced in the HEK monolayer. The cell samples were divided into two groups of CMC/TA and CMC/TA/Cu. Cells were cocultured with 300 μg mL^{-1} of CMC/TA and CMC/TA/Cu under weak acid cell medium for 0, 2, 4, and 6 h coculture at 37 °C and immediately digitally photographed.

2.5. Endothelial Tubule Stimulation. 2×10^5 Cells/well of human umbilical vein endothelia cells (HUVECs) were first added in a 24-well plate, followed by 12 h of incubation. Then, the prepared HUVECs were divided into two groups which were exposed to CMC/TA and CMC/TA/Cu hydrogels for 24 h with weak acid epithelial cell culture medium (ECM), respectively. Afterward, 50 μL/well, 2-fold free ECM-diluted Matrigel (BD Biosciences, USA) was slowly added into two 96-well plates; then, they were placed under a 37 °C incubator for 30 min. Subsequently, the above-treated HUVECs (1×10^4 cells/well) were collected and replated on the above BD gel-placed 96-well plate. The cells were incubated for another 2, 4, and 6 h. Finally, the enclosed mesh of the above-formed intact microtubes was imaged under an ordinary microscope, followed by the quantification of ImageJ.

2.6. Full-Thickness Wound with MRSA-Infected Model. Small animal studies were first conformed by the corresponding guidelines of animal care. All protocols for mammalian animal studies and the animal welfare were then approved by the Committee on the Ethics of Animal Experiments of Chinese Academy of Science with an approval

https://doi.org/10.1021/acsomega.3c06683
ACS Omega 2024, 9, 4386−4394

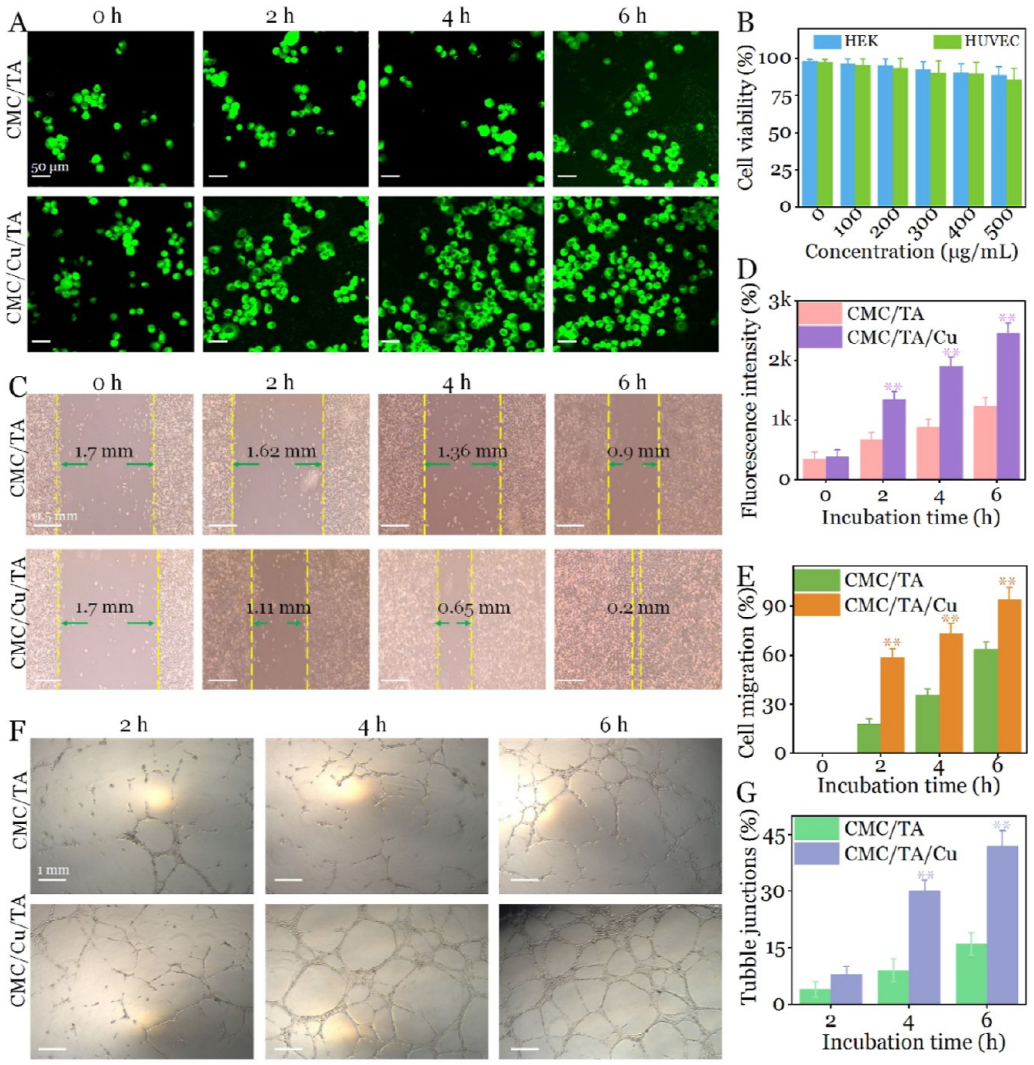

Figure 3. (A) Fluorescence images of HEK cells after immersion with CMC/TA and CMC/TA/Cu hydrogels for different hours. (B) HEK and HUVEC viabilities after immersion with various weights of CMC/TA/Cu hydrogels for 12 h. (C) Photographs of scratch assay of HEK cells after incubating with CMC/TA and CMC/TA/Cu hydrogels for various hours, respectively. (D) Qualification of the proliferation of HEK cells after treatments of CMC/TA and CMC/TA/Cu hydrogels. (E) In vitro cell migration percentage of HEK cells after various treatments. (F) Endothelial tubulogenesis evaluation in vitro. Digital photographs of HUVECs after treating with CMC/TA and CMC/TA/Cu hydrogels for various hours, respectively. (G) Quantification of the exact tubule junctions in the digital photographs of HUVECs after various treatments in F. "**" refers to $p < 0.05$.

number of 2020-01-01JiPi. MRSA-infected wounds are constructed using the following steps. The Balb/C mice were first anesthetized by isoflurane, the white hair on the back of hind legs were carefully shaved, and then depilatory cream was used to thoroughly scratch the fur clean. Then, full-thickness acute wounds were prepared by a miltex-biopsy perforator with a diameter of 6 mm. The MRSA-infected model was built according to the following procedure. The acute round wound was intramuscularly injected with a surface amplification of 100 μL of 2×10^7 CFU for 48 h.

2.7. In Vivo Repair of MRSA-Infected Wounds by CMC/TA/Cu Hydrogel. Balb/C mice with MRSA-infected full-thickness wounds were evenly divided into two groups: control group (PBS) and hydrogel group (CMC/TA/Cu) (7.5 mg/kg). Simultaneously, the full wound pictures were photographed every 3 days with PBS and CMC/TA/Cu treatments. The percentage of wound closure area was finally calculated by the conventional formula as follows

$$\%\ \text{Wound area closed} = \left(\frac{\text{wound area} \times \text{treated day}}{\text{wound area} \times \text{day 0}}\right) \times 100$$

2.8. In Vivo Antibacterial Evaluation. Furthermore, for the plate-counting strategy for antibacterial evaluation in vivo, MRSA infected wound tissues from CMC/TA and CMC/TA/Cu groups (triple administrations at days 0, 7, and 11). Then, the wound tissues were resected at day 1, day 8, and day 12, and all samples were immersed in PBS solution. After 2 h, the wound tissues were removed, and the obtained MRSA suspensions were diluted 1000 times by LB broth. Then, 100 μL of the diluted MRSA suspension of the two groups was spread on the solid LB medium and further incubated in an incubator (37 °C, 5% CO_2) for 24 h.

2.9. Histological Studies. For histological assay, finally, at day 12, mice from CMC/TA/Cu and PBS treatments were scarified; the wound tissues and main organs (heart, lung, liver,

https://doi.org/10.1021/acsomega.3c06683
ACS Omega 2024, 9, 4386−4394

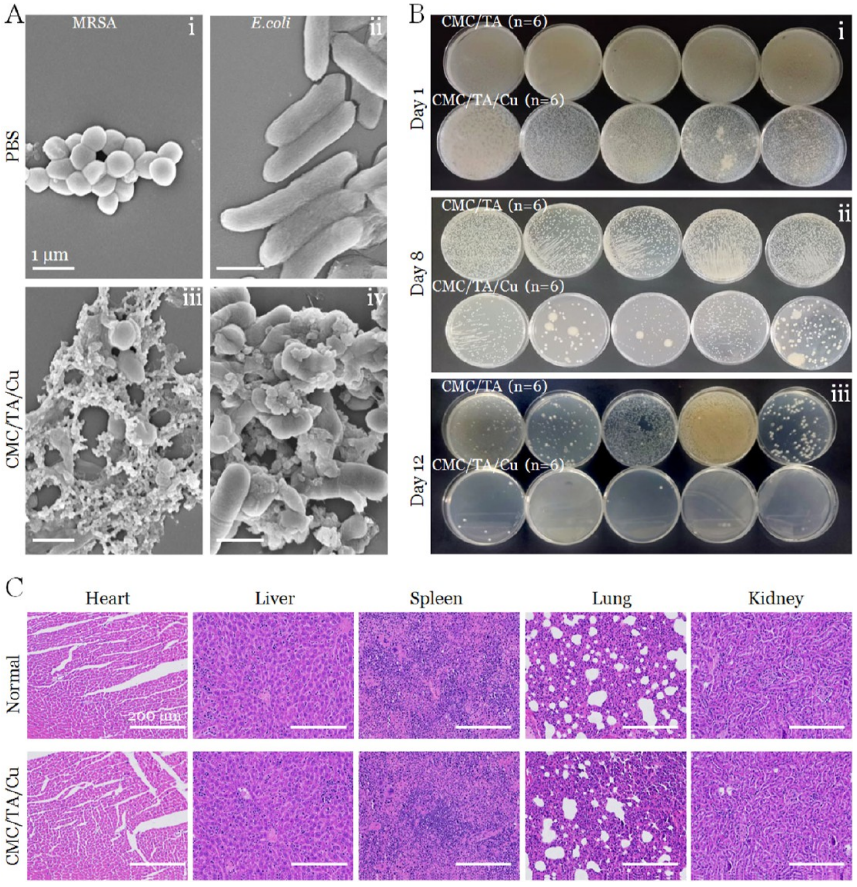

Figure 4. (A) SEM images of MRSA (i,iii) and *E. coli* (ii,iv) after incubating with PBS or CMC/TA/Cu for 2 h. (B) Photographs of MRSA colonies from wound tissue after treatment with CMC/TA/Cu and CMC/TA (n = 6) for day 1, day 8, and day 12, respectively. (C) H&E-analyzed images of the major organs in PBS or CMC/TA/Cu-treated Balb/c mice at day 12.

spleen, and kidney) were isolated and placed in a fixed solution of 4% of paraformaldehyde (1 mL). All the samples were cut in sections, and wound tissues and normal tissues were evaluated by H&E. Wounds were also assessed by Masson trichrome, immunohistochemical staining, as well as Giemsa staining.

3. RESULTS AND DISCUSSION

3.1. CMC/TA/Cu Fabrication and Characterization. In this work, with the buffering of sodium bicarbonate (4% w/v of $NaHCO_3$), 5% w/v of CMC and 0.3 g/mL TA could be rapidly cross-linked by the hydrogen bonds between the $-NH_2$ groups in CMC and −OH groups in TA. The formed CMC/TA hydrogel was first observed by SEM. It can be found that the synthesized CMC/TA hydrogel presented an interconnected microporous morphology with a diameter of 5−20 μm that facilitated the infiltration of both nutrients and oxygen (Figure 2Ai,Aii). Subsequently, as the Cu^{2+} precursor, the aqueous solution $CuCl_2$ (5% w/v) was introduced into the ingredients TA and $NaHCO_3$ that were codissolved in double-deionized H_2O. After adding CMC, the CMC/TA/Cu hydrogel was formed within 15 s. Obviously, due to the reaction $CuCl_2 + 2NaHCO_3 = Cu(OH)_2\downarrow + 2CO_2\uparrow + 2NaCl$, the in situ generated $Cu(OH)_2$ nanoparticles with size variation from nanoscale (∼100 nm) to microscale (∼1 μm) can be visualized in the SEM image of CMC/TA/Cu hydrogel (Figure 2Bi,Bii). The decorated Cu-based particles in the three-dimensional network structure could be ascribed to the strong coordination effect between the phenolic hydroxyl group and Cu^{2+}. Besides, after $Cu(OH)_2$ particles' loading, the size of the micropore is still maintained, primarily suggesting that the in situ reaction has a negligible effect on the mechanical properties of the hydrogel. Figure 2C shows the elemental mapping distribution on the surface of the CMC/TA/Cu hydrogel. Clearly, the Cu elemental signal was scattered well in the prepared hydrogel, testifying to the successful incorporation of $Cu(OH)_2$. Figure 2D illustrates the test of strain amplitude sweep; we found that at the junction of G' (storage modulus) and G'' (loss modulus) curve with a strain of 221%, the gel−sol transition occurred. This result was approximately close to the reported CMC/TA at a strain of 251%.[20] Furthermore, the efficiency of CMC/TA/Cu hydrolytic swelling was also monitored at 25 °C under PBS (1×). Apparently, the Cu-based hydrogel showed the analogous swelling property (17.11 ± 1.44 times) as CMC/TA hydrogel (16.84 ± 1.66 times) after 48 h of immersion (Figure 2E), further proving that the negligible pore size variation was induced after in situ production of $Cu(OH)_2$, and these interconnected porous morphologies exhibited exceptional water storage. Additionally, the release behaviors of Cu^{2+} and TA in the stimulated weak acid buffer (pH = 5.5) were also evaluated. As displayed in Figure 2F, both TA and Cu^{2+} were gradually released, and the maximum levels could reach after 24 h incubation. The comparable release features reflected that the CMC/TA/Cu hydrogel could concurrently deliver TA and Cu^{2+} to the biofilm in the initial phase of bacteria-infected wounds.

https://doi.org/10.1021/acsomega.3c06683
ACS Omega 2024, 9, 4386−4394

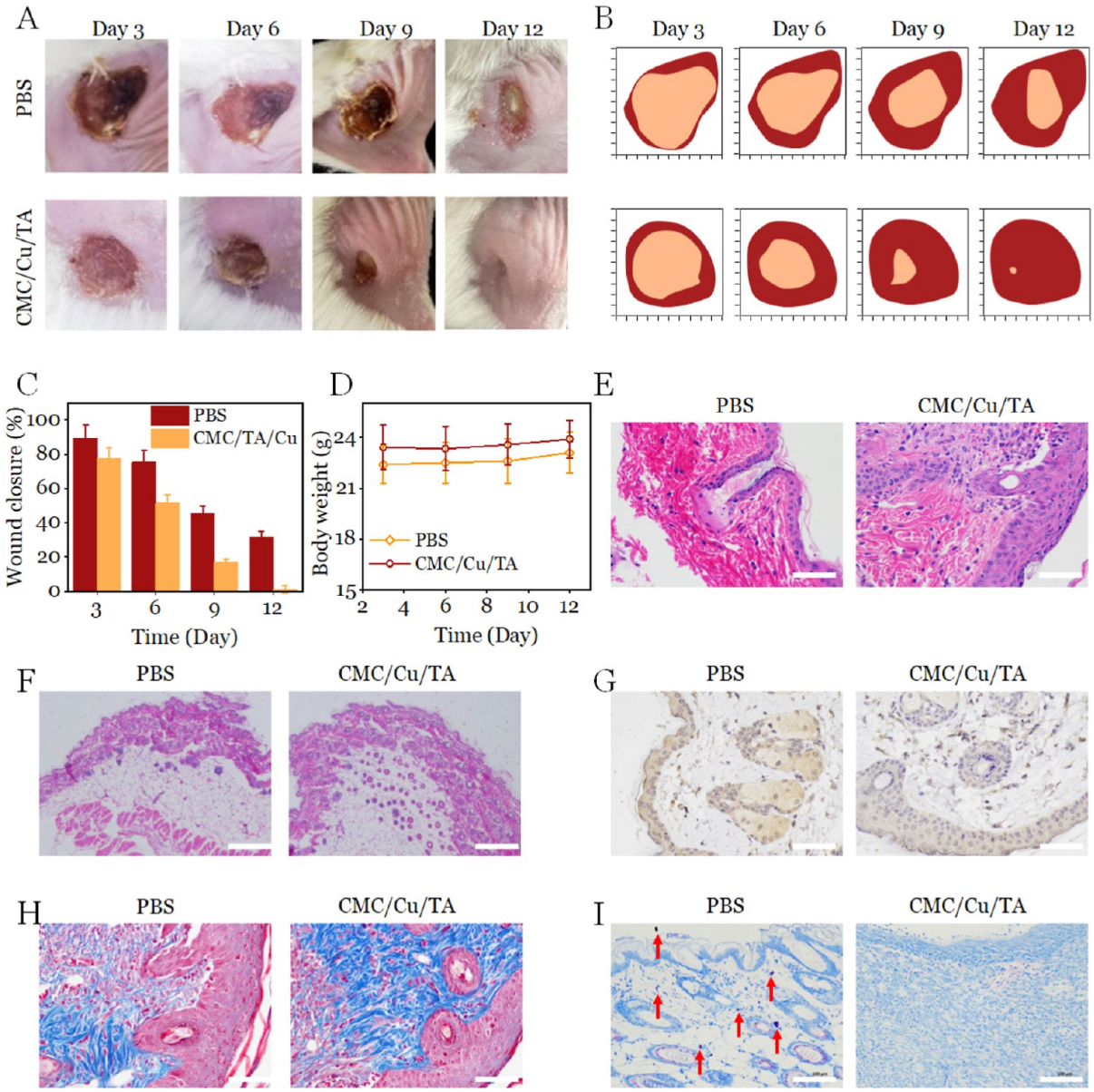

Figure 5. (A) Representative pictures of cutaneous wound with MRSA infection after treatment with PBS or CMC/TA/Cu hydrogel for various days. (B) Stimulated wound area traces after treatment with PBS or CMC/TA/Cu hydrogel for various days. (C) Wound closure rates and body weight (D) of the above two groups on days 3, 6, 9, and 12. H&E-stained photographs of (E) wound area and (F) newborn hair follicles after administration with PBS or CMC/TA/Cu hydrogel for 12 days. (G) Immunohistochemically stained (CD86-positive cells), (H) Masson's trichrome-stained, and (E) Giemsa-stained pictures of wound tissues after treatment with PBS or CMC/TA/Cu hydrogel for 12 days. Red arrows refer to a single MRSA. "*" refers to $p < 0.1$ and "**" refers to $p < 0.05$.

3.2. Proliferation and Migration of Keratinocyte and Angiogenesis of Endothelial Cells. The proliferation and migration of keratinocytes and the effective angiogenesis of endothelial cells play crucial roles in promoting the wound healing efficacy. First, the HEK cells and HUVECs showed ignorable cytotoxicity under different amounts of CMC/TA/Cu immersion for 24 h, confirming the superior biocompatibility of our prepared hydrogels toward normal tissue (Figure 3B). Because Cu^{2+} can mediate high-level expression of α_2, α_6, and β_1 integrins for stimulating the proliferation and migration of HEK, subsequently, the HEK proliferation (cultured in weak acid medium) of our Cu-based hydrogel was assessed. The wound dressing first adheres on the biofilm of the wound, in order to stimulate the bacteria-infected wound with weak acid condition on the outlayer, and accordingly, the two hydrogels were immersed in cell medium with pH at 5.5. Expectedly, in comparison with the CMC/TA group, keratinocyte cells immersed with CMC/TA/Cu indeed presented relatively 5 times higher proliferation rate (Figure 3A,D). It was significantly enhanced from 2 to 6 h. In contrast, the migration effect of HEK cells was monitored by a conventional scratch assay. Evidently, in sharp contrast with the migration rate of CMC/TA, that of CMC/TA/Cu hydrogel prominently promoted (Figure 3C). Correspondingly, the remarkable migration efficacy could be found at 2 h incubation of CMC/TA/Cu, and the scratch disappeared (94.2%) after 6 h of immersion, while still a large gap (63.7%) was discovered in CMC/TA-treated cells (Figure 3E). In the bargain, the gap distance of CMC/TA/Cu was 4.5-fold lower than that of CMC/TA at 6 h of treatment. Finally, the in vitro angiogenesis

https://doi.org/10.1021/acsomega.3c06683
ACS Omega 2024, 9, 4386−4394

feature in HUVECs was determined. Exhilaratingly, the tubulogenic effect in HUVECs exposed to the CMC/TA/Cu hydrogel for 6 h formed the maximum quantity of tubule junctions in comparison with HUVECs treated with CMC/TA (Figure 3F). Additionally, the counts of tubule nodes and mesh exhibited a similar trend in Cu-based hydrogel, exhibiting the maximum numbers when compared to CMC/TA (Figure 3G). The tubulogenic features of CMC/TA/Cu are expected to facilitate angiogenesis and promote wound healing in vivo. As expected, after 6 h administration of PBS, negligible HEK proliferation, migration, and tubulogenic effect of HUVECs were monitored (Figure S1). These findings were mainly due to sustainable Cu^{2+} release from the prepared Cu-based dressing.

3.3. High Anti-MRSA Efficiency In Vitro and In Vivo. In order to decipher the outstanding antibacterial ability of our hydrogel system, SEM was employed to investigate the detailed morphological variation of drug MRSA after treatment of PBS or CMC/TA/Cu for 2 h. As illustrated in Figure 4Ai,Aiii, untreated MRSA exhibited a typical globular structure with smooth surface and integrated cytoderm. Obviously, in the hydrogel-treated group, the cell wall was damaged, and all bacteria were destroyed with only fragmentation left. Additionally, a similar *E. coli* killing effect was also demonstrated with approximately the overall breakage (Figure 4Aii,Aiv). Furthermore, according to the LB plate data, bacterial killing rate could be significantly enhanced after 4 h treatment of CMC/TA/Cu, and in contrast with *E. coli*, a slightly higher eradication effect was presented in the MRSA group (Figure S2). In addition, to assess the anti-MRSA property of our novel hydrogel with in situ $Cu(OH)_2$ generation, the skin wound model was first constructed on right rear of back of Balb/c mice. Then, the MRSA dispersed PBS solution was intramuscularly injected and gently applied on the surface of wound before the day of various administrations. The mice were evenly divided into two groups: PBS and CMC/TA/Cu. To estimate the sterilization efficiency, the wound tissue from the above two groups were excised on days 1, 8, and 12 to apprise the exact number of MRSA. The results depicted in Figure 4B showed that in comparison with the CMC/TA-treated groups, the bacteria of CMC/TA/Cu could be significantly decreased, especially presenting the most efficacious bactericidal action with approximately 100% death at day 12. In parallel, for the group without $Cu(OH)_2$ loading, the live bacteria were 20 times higher than the CMC/TA/Cu-treated group (Figure S3). Undoubtedly, this data was mainly due to the Fenton reaction of Cu^{2+} for a large amount of reactive oxygen species generation and the antibacterial capacity of CMC and TA. Further, H&E staining assay of the main organs that resected at day 12 was conducted. Indeed, when compared to the healthy mice, the CMC/TA/Cu group presented no appreciable differences (Figure 4C), confirming the exceptional histocompatibility of our novel Cu-based hydrogel.

3.4. In Vivo MRSA-Infected Wound Repair by CMC/TA/Cu. Inspired by the aforementioned results, the wound healing capacity of the CMC/TA/Cu hydrogel was assessed on Balb/c mice with MRSA-infected wound tissue. Digital pictures were photographed for days 3, 6, 9, and 12 post-treatments of PBS and CMC/TA/Cu, respectively. In contrast with PBS-treated wounds, it was directedly discovered that the hydrogel group had more apparent wound shrinkage at each time point (Figure 5A). The wound closure traces and the corresponding wound closure rate suggested that the wound repair process of the PBS group was sustainably delayed. The wound area of the hydrogel-administered group was prominently reduced on day 9. Interestingly, the wound with hydrogel spraying was close to 80.12%, while that of the PBS-treated wounds presented only 54.31%. Particularly, after 12 days, the bacteria-infected wounds administrated with CMC/TA/Cu hydrogel were approximately recovered with newly generated skin tissues (98.13%), whereas wounds in the PBS group were not yet repaired with large scabs (70.12%). Additionally, the body weight of the two groups had undetectable fluctuation during the restoration period, further demonstrating the biosafety in vivo. In the end, the wounds were conducted by various pathological analysis. As illustrated in H&E-stained images, the hydrogel therapy group presented an intact and thick epidermal layer with massive cells immersing and regenerated hair follicles, while the control group still had incomplete and thin epithelium with little hair follicles (Figure 5E,F). As the maker of M1 macrophage that is typically presented in wounds, the distribution of CD86-positive cells was evaluated by immunohistochemical analysis. Notably, the inflammation level in the hydrogel group was remarkably alleviated (Figure 5G). Masson trichrome-stained studies demonstrated higher nascent collagen deposition in the newly generated skin tissue when treated with CMC/TA/Cu hydrogel (Figure 5H). Both the findings roughly agreed with H&E results. Then, the residual bacteria in the wounds were apprised by Giemsa-stained studies. As shown in Figure 5I, a large number of MRSA (red arrows) were revealed in the corresponding PBS group, whereas scarcely any bacteria could be detected in the CMC/TA/Cu hydrogel group. Convincingly, this finding was consistent with the in vitro anti-MRSA result (Figure 4A,B). All the in vivo discovery testified that the CMC/TA/Cu hydrogel presented immense prospect for accelerating wound repair in clinic.

4. CONCLUSIONS

In summary, a novel hydrogel depending on CMC, TA, and in situ $Cu(OH)_2$ generation was synthesized through hydrogen bonding and ion coordination. The hydrogel could promote migration and proliferation of keratinocytes and stimulate angiogenesis of endothelial cells. Further, owing to the antibacterial abilities of CMC, TA, and $Cu(OH)_2$, it presented an outstanding MRSA elimination effect both in vitro and in vivo. Additionally, in the full-thickness and MRSA-infected wound model, CMC/TA/Cu hydrogel had an effective therapeutic impact on the regeneration of newborn hair follicles, remodeling of epidermal, deposition of collagen, as well as alleviation of inflammatory level. Combined with the superior biocompatibility and low adverse side effect, our Cu-based hydrogel was a feasible alternation for the advancement of repair the full-thickness wound with bacteria infected in clinic.

■ ASSOCIATED CONTENT

Supporting Information

The Supporting Information is available free of charge at https://pubs.acs.org/doi/10.1021/acsomega.3c06683.

Description of the materials used and exact number of MRSA in wound tissues (PDF)

https://doi.org/10.1021/acsomega.3c06683
ACS Omega 2024, 9, 4386−4394

AUTHOR INFORMATION

Corresponding Authors

Peiyuan Wang − *Key Laboratory of Design and Assembly of Functional Nanostructures, Fujian Institute of Research on the Structure of Matter, Chinese Academy of Sciences, Fuzhou 350002, P. R. China; College of Life Sciences, Fujian Agriculture and Forestry University, Fuzhou 350002, China;* orcid.org/0000-0003-1700-1061; Email: wangpeiyuan@fjirsm.ac.cn

Xiaolong Liu − *Key Laboratory of Design and Assembly of Functional Nanostructures, Fujian Institute of Research on the Structure of Matter, Chinese Academy of Sciences, Fuzhou 350002, P. R. China; College of Life Sciences, Fujian Agriculture and Forestry University, Fuzhou 350002, China; The United Innovation of Mengchao Hepatobiliary Technology Key Laboratory of Fujian Province, Mengchao Hepatobiliary, Hospital of Fujian Medical University, Fuzhou 350025, P. R. China;* orcid.org/0000-0002-3096-4981; Email: xiaoloong.liu@gmail.com

Authors

Jinhui Lin − *Key Laboratory of Design and Assembly of Functional Nanostructures, Fujian Institute of Research on the Structure of Matter, Chinese Academy of Sciences, Fuzhou 350002, P. R. China; College of Life Sciences, Fujian Agriculture and Forestry University, Fuzhou 350002, China*

Siyaqi Li − *Key Laboratory of Design and Assembly of Functional Nanostructures, Fujian Institute of Research on the Structure of Matter, Chinese Academy of Sciences, Fuzhou 350002, P. R. China; College of Life Sciences, Fujian Agriculture and Forestry University, Fuzhou 350002, China*

Yunfei Ying − *Key Laboratory of Design and Assembly of Functional Nanostructures, Fujian Institute of Research on the Structure of Matter, Chinese Academy of Sciences, Fuzhou 350002, P. R. China; Department of Biochemistry and Molecular Biology, the Key Laboratory of Ecological Environment and Critical Human Diseases Prevention of Hunan Province Department of Education, Hunan Province Cooperative Innovation Center for Molecular Target New Drug Study, School of Basic Medicine, University of South China, Hengyang 421001, P. R. China*

Weilin Zheng − *School of Medicine and School of Biomedical Sciences, Huaqiao University, Quanzhou, Fujian 362021, China*

Jingcheng Wu − *Department of Health Science, Technology and Education, National Health Commission of the People's Republic of China, Beijing 100088, China*

Complete contact information is available at: https://pubs.acs.org/10.1021/acsomega.3c06683

Author Contributions

J.L. contributed to methodology, investigation, formal analysis, data curation, and writing original draft. S.L. contributed to investigation, validation, and data curation. Y.Y. contributed to methodology and supervision. W.Z. contributed to investigation and visualization. J.W. contributed to investigation and visualization. P.W. contributed to conceptualization, writing—review and editing, and project administration. X.L. contributed to supervision, writing—review and editing, resources, project administration, and funding acquisition. J.L. and S.L. contributed equally to this work.

Notes

The authors declare no competing financial interest.

ACKNOWLEDGMENTS

The authors acknowledge funding from the Special Fund Project for Fujian Marine Economic Development in 2022 (no. FJHJF-L-2022-2), the XMIREM autonomously deployment project (2023CX12), and a Research Fund of Fujian Key Laboratory of Precision Diagnosis and Treatment in Breast Cancer & Xiamen Key Laboratory of Xiamen Key Laboratory of Endocrine-Related Cancer Precision Medicine (XKLEC2021KF04).

REFERENCES

(1) Schultz, G. S.; Sibbald, R. G.; Falanga, V.; Ayello, E. A.; Dowsett, C.; Harding, K.; Romanelli, M.; Stacey, M. C.; Teot, L.; Vanscheidt, W. Wound bed preparation: a systematic approach to wound management. *Wound Repair Regen.* **2003**, *11*, S1−S28.

(2) Zhong, S. P.; Zhang, Y. Z.; Lim, C. T. Tissue scaffolds for skin wound healing and dermal reconstruction. *Wiley Interdiscip. Rev.: Nanomed. Nanobiotechnol.* **2010**, *2*, 510−525.

(3) Pereira, R.; Carvalho, A.; Vaz, D. C.; Gil, M. H.; Mendes, A.; Bártolo, P. Development of novel alginate based hydrogel films for wound healing applications. *Int. J. Biol. Macromol.* **2013**, *52*, 221−230.

(4) Xu, C.; Akakuru, O. U.; Ma, X.; Zheng, J.; Zheng, J.; Wu, A. Nanoparticle-Based Wound Dressing: Recent Progress in the Detection and Therapy of Bacterial Infections. *Bioconjugate Chem.* **2020**, *31*, 1708−1723.

(5) Dhivya, S.; Padma, V. V.; Santhini, E. Wound dressings-a review. *BioMedicine* **2015**, *5*, 22.

(6) Nguyen, H. M.; Ngoc Le, T. T.; Nguyen, A. T.; Thien Le, H. N.; Pham, T. T. Biomedical materials for wound dressing: recent advances and applications. *RSC Adv.* **2023**, *13*, 5509−5528.

(7) Gruppuso, M.; Turco, G.; Marsich, E.; Porrelli, D. Polymeric wound dressings, an insight into polysaccharide-based electrospun membranes. *Appl. Mater. Today* **2021**, *24*, 101148.

(8) Weller, C.; Sussman, G. Wound dressings update. *J. Pharm. Pract. Sci.* **2006**, *36*, 318−324.

(9) Zhong, Y.; Xiao, H.; Seidi, F.; Jin, Y. Natural polymer-based antimicrobial hydrogels without synthetic antibiotics as wound dressings. *Biomacromolecules* **2020**, *21*, 2983−3006.

(10) Pourshahrestani, S.; Zeimaran, E.; Kadri, N. A.; Mutlu, N.; Boccaccini, A. R. Polymeric hydrogel systems as emerging biomaterial platforms to enable hemostasis and wound healing. *Adv. Healthcare Mater.* **2020**, *9*, 2000905.

(11) Wang, C.; Wang, M.; Xu, T.; Zhang, X.; Lin, C.; Gao, W.; Xu, H.; Lei, B.; Mao, C. Engineering bioactive self-healing antibacterial exosomes hydrogel for promoting chronic diabetic wound healing and complete skin regeneration. *Theranostics* **2019**, *9*, 65−76.

(12) He, Y.; Zhao, W.; Dong, Z.; Ji, Y.; Li, M.; Hao, Y.; Zhang, D.; Yuan, C.; Deng, J.; Zhao, P.; Zhou, Q. A biodegradable antibacterial alginate/carboxymethyl chitosan/Kangfuxin sponges for promoting blood coagulation and full-thickness wound healing. *Int. J. Biol. Macromol.* **2021**, *167*, 182−192.

(13) Li, H.; Zhou, X.; Luo, L.; Ding, Q.; Tang, S. Bio-orthogonally crosslinked catechol-chitosan hydrogel for effective hemostasis and wound healing. *Carbohydr. Polym.* **2022**, *281*, 119039.

(14) Li, M.; Liang, Y.; He, J.; Zhang, H.; Guo, B. Two-pronged strategy of biomechanically active and biochemically multifunctional hydrogel wound dressing to accelerate wound closure and wound healing. *Chem. Mater.* **2020**, *32*, 9937−9953.

(15) Chien, R.-C.; Yen, M.-T.; Mau, J.-L. Antimicrobial and antitumor activities of chitosan from shiitake stipes, compared to commercial chitosan from crab shells. *Carbohydr. Polym.* **2016**, *138*, 259−264.

(16) Tsurkan, M. V.; Voronkina, A.; Khrunyk, Y.; Wysokowski, M.; Petrenko, I.; Ehrlich, H. Progress in chitin analytics. *Carbohydr. Polym.* **2021**, *252*, 117204.
(17) Jones, M.; Kujundzic, M.; John, S.; Bismarck, A. Crab *vs.* mushroom: A review of crustacean and fungal chitin in wound treatment. *Mar. Drugs* **2020**, *18*, 64.
(18) Deng, L.; Zhang, L.-M. Rheological characteristics of chitin/ionic liquid gels and electrochemical properties of regenerated chitin hydrogels. *Colloids Surf., A* **2020**, *586*, 124220.
(19) Liu, H.; Yang, Q.; Zhang, L.; Zhuo, R.; Jiang, X. Synthesis of carboxymethyl chitin in aqueous solution and its thermo-and pH-sensitive behaviors. *Carbohydr. Polym.* **2016**, *137*, 600−607.
(20) Zhou, X.; Zhou, Q.; Chen, Q.; Ma, Y.; Wang, Z.; Luo, L.; Ding, Q.; Li, H.; Tang, S. Carboxymethyl Chitosan/Tannic Acid Hydrogel with Antibacterial, Hemostasis, and Antioxidant Properties Promoting Skin Wound Repair. *ACS Biomater. Sci. Eng.* **2023**, *9*, 437−448.
(21) Liao, J.; Hou, B.; Huang, H. Preparation, properties and drug controlled release of chitin-based hydrogels: An updated review. *Carbohydr. Polym.* **2022**, *283*, 119177.
(22) Zhao, X.; Zhou, L.; Li, Q.; Zou, Q.; Du, C. Biomimetic mineralization of carboxymethyl chitosan nanofibers with improved osteogenic activity in vitro and *in vivo*. *Carbohydr. Polym.* **2018**, *195*, 225−234.
(23) Wang, D.; Zhang, N.; Meng, G.; He, J.; Wu, F. The effect of form of carboxymethyl-chitosan dressings on biological properties in wound healing. *Colloids Surf., B* **2020**, *194*, 111191.
(24) Wang, Y.-L.; Zhou, Y.-N.; Li, X.-Y.; Huang, J.; Wahid, F.; Zhong, C.; Chu, L.-Q. Continuous production of antibacterial carboxymethyl chitosan-zinc supramolecular hydrogel fiber using a double-syringe injection device. *Int. J. Biol. Macromol.* **2020**, *156*, 252−261.
(25) Upadhyaya, L.; Singh, J.; Agarwal, V.; Tewari, R. P. The implications of recent advances in carboxymethyl chitosan based targeted drug delivery and tissue engineering applications. *J. Controlled Release* **2014**, *186*, 54−87.
(26) Huang, Y.; Mu, L.; Zhao, X.; Han, Y.; Guo, B. Bacterial Growth-Induced Tobramycin Smart Release Self-Healing Hydrogel for Pseudomonas aeruginosa-Infected Burn Wound Healing. *ACS Nano* **2022**, *16*, 13022−13036.
(27) Quideau, S.; Deffieux, D.; Douat-Casassus, C.; Pouységu, L. Plant polyphenols: chemical properties, biological activities, and synthesis. *Angew. Chem., Int. Ed.* **2011**, *50*, 586−621.
(28) Gülçin, İ.; Huyut, Z.; Elmastaş, M.; Aboul-Enein, H. Y. Radical scavenging and antioxidant activity of tannic acid. *Arabian J. Chem.* **2010**, *3*, 43−53.
(29) Chung, K.-T.; Wong, T. Y.; Wei, C.-I.; Huang, Y.-W.; Lin, Y. Tannins and Human Health: A Review. *Crit. Rev. Food Sci. Nutr.* **1998**, *38*, 421−464.
(30) Yang, J.; Li, M.; Wang, Y.; Wu, H.; Zhen, T.; Xiong, L.; Sun, Q. Double Cross-Linked Chitosan Composite Films Developed with Oxidized Tannic Acid and Ferric Ions Exhibit High Strength and Excellent Water Resistance. *Biomacromolecules* **2019**, *20*, 801−812.
(31) Chen, Y.-N.; Peng, L.; Liu, T.; Wang, Y.; Shi, S.; Wang, H. Poly(vinyl alcohol)-Tannic Acid Hydrogels with Excellent Mechanical Properties and Shape Memory Behaviors. *ACS Appl. Mater. Interfaces* **2016**, *8*, 27199−27206.
(32) Payne, D. E.; Martin, N. R.; Parzych, K. R.; Rickard, A. H.; Underwood, A.; Boles, B. R. Tannic Acid Inhibits *Staphylococcus aureus* Surface Colonization in an IsaA-Dependent Manner. *Infect. Immun.* **2013**, *81*, 496−504.
(33) Chang, C.-Y.; Krishnan, T.; Wang, H.; Chen, Y.; Yin, W.-F.; Chong, Y.-M.; Tan, L. Y.; Chong, T. M.; Chan, K.-G. Non-antibiotic quorum sensing inhibitors acting against N-acyl homoserine lactone synthase as druggable target. *Sci. Rep.* **2014**, *4*, 7245.
(34) Cámara, M.; Williams, P.; Hardman, A. Controlling infection by tuning in and turning down the volume of bacterial small-talk. *Lancet Infect. Dis.* **2002**, *2*, 667−676.
(35) Khan, N. S.; Ahmad, A.; Hadi, S. M. Anti-oxidant, pro-oxidant properties of tannic acid and its binding to DNA. *Chem.-Biol. Interact.* **2000**, *125*, 177−189.
(36) Shutova, T. G.; Agabekov, V. E.; Lvov, Y. M. Reaction of radical cations with multilayers of tannic acid and polyelectrolytes. *Russ. J. Gen. Chem.* **2007**, *77*, 1494−1501.
(37) Ge, S.; Ji, N.; Cui, S.; Xie, W.; Li, M.; Li, Y.; Xiong, L.; Sun, Q. Coordination of covalent cross-linked gelatin hydrogels *via* oxidized tannic acid and ferric ions with strong mechanical properties. *J. Agric. Food Chem.* **2019**, *67*, 11489−11497.
(38) Zhu, S.; Zhao, B.; Li, M.; Wang, H.; Zhu, J.; Li, Q.; Gao, H.; Feng, Q.; Cao, X. Microenvironment responsive nanocomposite hydrogel with NIR photothermal therapy, vascularization and anti-inflammation for diabetic infected wound healing. *Bioact. Mater.* **2023**, *26*, 306−320.
(39) Li, Q.; Song, H.; Li, S.; Hu, P.; Zhang, C.; Zhang, J.; Feng, Z.; Kong, D.; Wang, W.; Huang, P. Macrophage metabolism reprogramming EGCG-Cu coordination capsules delivered in polyzwitterionic hydrogel for burn wound healing and regeneration. *Bioact. Mater.* **2023**, *29*, 251−264.
(40) Ye, L.; He, X.; Obeng, E.; Wang, D.; Zheng, D.; Shen, T.; Shen, J.; Hu, R.; Deng, H. The CuO and AgO co-modified ZnO nanocomposites for promoting wound healing in *Staphylococcus aureus* infection. *Mater. Today Bio* **2023**, *18*, 100552.
(41) Li, D.; Li, J.; Wang, S.; Wang, Q.; Teng, W. Dually Crosslinked Copper-Poly(tannic acid) Nanoparticles with Microenvironment-Responsiveness for Infected Wound Treatment. *Adv. Healthcare Mater.* **2023**, *12* (17), 2203063.
(42) Di Nardo, T.; Hadad, C.; Nguyen Van Nhien, A.; Moores, A. Synthesis of high molecular weight chitosan from chitin by mechanochemistry and aging. *Green Chem.* **2019**, *21*, 3276−3285.

https://doi.org/10.1021/acsomega.3c06683
ACS Omega 2024, 9, 4386−4394